Hazard assessment for typhoon-induced coastal flooding and inundation in Shanghai, China

Jie Yin[1,2,3], Ning Lin[2*], Yuhan Yang[1], William J. Pringle[4], Joannes J. Westerink[4], Dapeng Yu[5]

1 Key Laboratory of Geographic Information Science (Ministry of Education), East China Normal University, China

2 Department of Civil and Environmental Engineering, Princeton University, USA

3 Institute of Eco-Chongming, East China Normal University, China

4 Department of Civil and Environmental Engineering and Earth Sciences, University of Notre Dame, IN, USA

5 Department of Geography, Loughborough University, UK

* Correspondence to: N.L. (email: nlin@princeton.edu)

Abstract: This paper describes an integrated statistical-hydrodynamic method to estimate tropical cyclone-induced coastal flood inundation hazard, applied to a coastal megacity-Shanghai, China. We identify three "worst-case" scenarios (extracted from over 5000 synthetic storms) that generate unprecedentedly high flood levels in Shanghai. Nevertheless, we find that the mainland Shanghai is relatively safe from coastal flooding under the current climate, thanks to its high-standard seawall protection. However, the city is expected to be increasingly at risk due to future sea level rise, with inundation two times and 20 times more likely to occur by mid- and late-21st century, respectively, and inundation depth and area to greatly increase (e.g., 60-1360% increase in the inundation area for the "worst cases" by 2100). The low-lying and poorly-protected area (e.g. Chongming island) is likely to be moderately affected by flood events with long return periods at the current state but could be largely inundated in future sea-level-rise situations.

Key Points:

1. An integrated statistical-hydrodynamic method is developed to estimate tropical cyclone-induced coastal flood inundation hazard.
2. The mainland Shanghai is found to be well protected by high-standard seawalls.
3. However, Shanghai is expected to be increasingly at risk due to future sea level rise.

Key Words: Topical Cyclone, Storm Tide, Inundation, Sea Level Rise, Flood Protection, Shanghai

Plain Language Summary: Coastal flooding associated with tropical cyclones (TCs, also called typhoons in the Northwest Pacific Basin) is often the most devastating and costliest of natural hazards. Struck by a number of strong TCs in recorded history, Shanghai may be highly vulnerable to coastal flooding due to its location within the Yangtze River delta, low-relief topography and high-density population. However, given the limited historical data, observation-based analysis is insufficient to capture the potential extreme events. In this study, we use a synthetic storm model to generate large numbers of TC events that are physically plausible but may have never occurred in the past. Storm tide and the resultant coastal flooding induced by each TC are further simulated with a coupled circulation-inundation model. Results suggest that Shanghai may encounter extreme storm tide flooding with very low possibilities under the current climate condition. With the protection of seawall, the city is generally immune to extensive flooding, except the low-lying and poorly-protected coastal floodplain and estuarine island, Chongming. However, future sea level rise will induce a significantly increased flood risk in Shanghai over the 21st century.

1. Introduction

Tropical cyclones (TCs), associated with extreme wind, rainfall and storm surge, are responsible for significant property damage and loss of life in coastal areas (Smith and Katz, 2013). Often, TC-induced storm surge together with astronomical high tide have been suggested as the primary causes of episodic flooding in low-lying coastal regions. Recent flood catastrophes illustrate that coastal cities, as the agglomeration of population and assets, are particularly vulnerable to storm tide flooding. For example, the unprecedented flooding of New Orleans due to Hurricane Katrina (2005) caused hundreds of fatalities and more than $40 billion in economic losses, making it the worst natural disaster in U.S. history (Kates et al., 2006). Hurricane Sandy (2012) resulted in the deaths of tens of people due to drowning and at least $20 billion in flood-related damages in New York City (Blake et al., 2013). Coastal flooding is expected to be more frequent and devastating, owing to rapid urbanization, sea level rise (SLR) and TC intensification in a warming climate (Emanuel, 2013; Woodruff et al., 2013; Hallegatte et al., 2013; Lin and Shullman 2017; Vitousek et al., 2017; Marsooli et al. 2019; Knutson et al., 2020). Hence, it is essential to quantify TC-induced flood hazards at city or regional scales.

To ensure an accurate assessment of TC-induced flood hazards for coastal cities, a large number of TC events are required particularly for addressing extreme flood hazards induced by low-probability storms. Due to the lack of sufficient measurements over a long period, statistical methods have been commonly used to generate large samples of synthetic TCs for a specific site (e.g., a city) of interest (Batts et al., 1980; Georgiou et al., 1983). The basic idea of these models is that probability distributions of key TC parameters (e.g., central pressure and radius of maximum wind) are fitted to the historical record, and then a Monte Carlo approach is applied to sample from these distributions. To overcome the limitation of local data, Vickery et al. (2000, 2009) applied the basin-wide data to develop a probabilistic track model with TC intensity along the track

estimated based on storm persistent and environmental variables such as the sea surface temperature. Furthermore, Emanuel et al. (2008), Lee et al. (2018), and Jing and Lin (2020) developed more advanced probabilistic track models by incorporating more environmental and oceanic variables that are essential to storm development. The advent of synthetic TC simulation has enabled probabilistic TC hazard assessment for coastal cities.

Recently, synthetic TC simulation has been increasingly used to drive storm tide simulation and assess flood hazards at the city scale. Lin et al. (2010, 2012, 2016) applied the statistical-deterministic model developed by Emanuel et al. (2008) to produce large numbers of synthetic storms for New York City (NYC), and then they used two hydrodynamic models: the Sea, Lake and Overland Surges from Hurricanes (SLOSH) model (Jelesnianski et al., 1992) and the Advanced Circulation (ADCIRC) model (Luettich et al., 1992; Westerink et al., 1994) with a high resolution mesh (up to 10 m around NYC) to simulate storm surges and storm tides induced by synthetic TCs. They estimated the probabilistic distribution of storm tides along NYC coast and found a heavy tail for very low occurrence probability events. Furthermore, the simulated surge heights along the coast from Lin et al. (2012) were interpolated and applied to terrain elevation for determining the flood inundation (extent and depth) and associated probabilities for NYC (Aerts et al., 2013). However, the simple nearest neighbor extrapolation method used in this analysis does not consider the dynamic nature of flood routing and may cause biases in the final inundation maps (Barnard et al., 2019). More recently, Yin et al. (2016) described a new method for coastal flood simulation by coupling ADCIRC and a simplified 2D flood inundation model (FloodMap) and applied the analysis to NYC for the case of Hurricane Sandy. The coupled model demonstrated efficiency and improved prediction over ADCIRC-only simulations for estimating storm-induced flooding in coastal areas.

In this study, an integrated statistical-hydrodynamic approach is proposed by running the statistical-deterministic hurricane model, ADCIRC, and FloodMap in sequence, to derive probabilistic flood hazard maps and to investigate possible worst-case flood scenarios for coastal cities under the current climate conditions as well as projected future SLR scenarios. To our knowledge, this study is the first that couples probabilistic hurricane model, storm surge model, inundation model, coastal protection data, and SLR projections to quantify the inundation hazards (probabilities). The proposed approach is applied to analyze the coastal flood hazard for the city of Shanghai, which is within the Northwest Pacific Basin and is highly exposed to typhoon-induced coastal flooding. For instance, Typhoon Winnie (1997) caused storm tides up to nearly 7 meters above Wusong Datum, the highest recorded in Shanghai's history. Meanwhile, Shanghai is protected by high-standard flood defense, which needs to be taken into account when estimating the inundation risk and effects of SLR. The remainder of this paper is organized as follows. Section 2 describes materials and methods, including synthetic TC dataset, storm tide simulation, flood probability analysis, and coastal inundation modeling. Section 3 presents the results and discusses the key findings. Section 4 provides the conclusions and offers suggestions for further research.

2. Materials and Methodology

2.1. Historical Events and Flood Protection of Shanghai

Shanghai has witnessed frequent extreme flooding induced by TCs. 148 TCs affected the region from 1949 to 2015 (Wang et al., 2017), among which 19 and 72 TCs generated storm surges of higher than 1.2 and 0.8 m, respectively. The annual maximum water levels (Fig. S1) were generally caused by the high tides and storm

surges. For example, the arrival of Typhoon Winnie's peak surge (2.35 m) coincided with the high astronomical tide, resulting in the highest storm tide (5.99 m) on record in Shanghai. In response to rising record levels, a flood defense system (floodwall along Huangpu River and seawall along the coast) was initiated in 1950s and has been reinforced since then (Fig. S1). Each update of protection standard is triggered by an extreme TC flood event (i.e., typhoons in 1962, 1974, 1981 and 1997), which heavily inundated the city (Xian et al., 2018). At present, Shanghai is protected by 480-km high level (1000-years) floodwalls and 508-km high standard seawalls which are designed to withstand a 100/200-year storm tides plus waves induced by 11/12-force winds (Saffir-Simpson Hurricane Category 1). In addition, rainfalls and river discharges are regulated by storm sewer drainage network and the dams/barriers/sluice gates, in order to prevent the compounding effects of pluvial, fluvial and coastal flooding (Yin et al, 2015; Xian et al, 2018).

2.2. Synthetic TC Dataset

To overcome the limitation of historical data, we estimate TC-induced coastal flood and inundation hazard based on large numbers of synthetic storms. We apply a synthetic TC dataset generated by the deterministic-statistical TC model of Emanuel et al. (2008). This model uses thermodynamic and kinematic statistics of the atmosphere and ocean derived from reanalysis data or climate-model estimation to produce synthetic TCs; it has been widely used to study hurricane wind, storm surge, and rainfall hazards (e.g., Emanuel 2017, Marsooli et al. 2019). Specifically, Xu et al. (2020) applied the synthetic TC model to study typhoon wind hazard for the Shanghai area. We apply the synthetic TC dataset generated in Xu et al. (2020) for the climate over the period of 1979 ~ 2015 based on the National Centers for Environmental Prediction (NCEP) reanalysis (Kalnay et al. 1996). The dataset includes 5018 synthetic storms. Each synthetic storm passes within a 350-

136 km-radius circle centered at a point near Shanghai (latitude 29.86° and longitude 121.56°), and all storms pass
137 within this circle with the maximum wind intensity (1-min wind speed at 10 m above sea level) greater than
138 21 m/s (40 knots). Each storm is characterized by 2-hourly time series of the storm parameters (i.e., time,
139 center position, maximum wind speed, pressure deficit, and radius of maximum wind) required for storm tide
140 modeling. The annual storm frequency associated with the storm set is about 2 storms per year. Xu et al.
141 (2020) found that the estimated wind hazard based on the NCEP synthetic dataset compared well with
142 historical wind observations in the Shanghai region.
143
144 **2.3. Storm Tide Simulation**
145
146 We use the ADvanced CIRCulation model (ADCIRC) to simulate storm tides (i.e., the total water level
147 including storm surge and astronomical tide). ADCIRC, originally developed by Luettich et al. (1992) and
148 Westerink et al. (1994), is a well-established open-source hydrodynamic model applicable to free surface
149 circulation and transport problems. The model adopts the hydrostatic pressure assumption to numerically
150 solve the governing equations in space and time using, respectively, the finite-element and finite-difference
151 numerical methods. ADCIRC solves the 2-D or 3-D momentum equations to calculate velocity fields. For
152 storm surge modeling in the coastal ocean, the 2-D depth-integrated model is usually preferred to the 3-D
153 model because it is computationally cheaper and largely captures the dominant processes that control the
154 storm-induced water level (Resio and Westerink, 2008). In the present study, we use the 2-D depth-integrated
155 version of ADCIRC. Due to the extremely large computational resource that would be required to simulate
156 wind waves associated with the large number of synthetic storms, we do not apply wave simulations here.
157 Thus we neglect the effect of wave setup on the total water level, which has been estimated to contribute up to

158 10-20% to total extreme water levels in the Shanghai region (Melet et al., 2018).

159

160 Using the mesh generation module of Surface-water Modeling System (SMS), we develop a computational
161 mesh that extends between latitudes 21°N and 41°N and longitudes 116.5°W and 129.5°W. The computational
162 domain consists of an unstructured triangular mesh with 108,440 nodes and 209,844 elements. The mesh
163 resolution is <100 m nearshore and gradually increases to > 50 km in deeper waters. The bathymetry of the
164 model is based on the bathymetry survey of Yangtze River Estuary in 2012 (Zhu and Bao, 2016) and GEBCO
165 (GEneral Bathymetric Chart of the Oceans)-2014 global 30 arc sec gridded data
166 (https://www.gebco.net/data_and_products/historical_data_sets/). The vertical datum is in mean sea level
167 (referenced to year 2000). The manning's n bottom roughness coefficient varies spatially over the grid based
168 on a global database for sediments on the seabed (http://portal.gplates.org/static/html/seafloor.html). The
169 water level at the open boundaries is specified by eight major tidal constituents (K1, K2, M2, N2, O1, P1, Q1,
170 and S2). The tidal information, including the amplitudes and phases, are obtained from the global model of
171 ocean tides TPXO8-ATLAS with a $1/30^{\circ}$ resolution (Egbert and Erofeeva, 2002). At closed boundaries, i.e.,
172 island and mainland shorelines, the normal flow is set to zero whereas the tangential velocity is determined
173 based on the free-slip boundary condition. While it is difficult to validate the ADCIRC modeling for storm
174 surges in Shanghai, as a critical TC parameter --radius of maximum wind--is not available in the historical
175 record for the Northwest Pacific Basin, the ADCIRC model has been found to produce storm surge
176 estimations with relatively high accuracy in a number of studies (e.g., Westerink et al., 2008; Marsooli and
177 Lin, 2018). Our evaluation on the model performance in simulating the astronomical tides, which can
178 contribute to over 75% of the storm tides in Shanghai, shows that the ADCIRC model satisfactorily captures
179 the dominant dynamics of major tide constituents along the Shanghai coast (Fig. S2).

We use analytical/parametric models to calculate the surface wind and pressure fields associated with the synthetic TCs to drive the hydrodynamic modeling. We use the parametric model of Holland (1980) to calculate the radial profile of pressure, which is related to the maximum wind speed, radius of maximum wind, and pressure deficit. We use the analytical model of Emanuel and Rotunno (2011) to calculate the wind field. The model calculates the 1-min axisymmetric wind field (associated with the storm) at the gradient level based on the storm characteristics including maximum wind speed and radius of maximum wind. We convert the gradient wind to the surface level (10 m above the sea surface) with a velocity reduction factor of 0.85 (Georgiou et al., 1983) and an empirical expression of inflow angles (Bretschneider, 1972). We add to the storm wind the surface environmental wind estimated as a fraction (0.55, rotated counter-clockwise by 20°) of the storm translation velocity, to account for the asymmetry of the wind field (Lin and Chavas, 2012). Finally, for use in the ADCIRC modeling we adjust the 1-minute wind to a 10-minute average with a reduction factor of 0.893 (Powell et al., 1996). This framework of TC modeling for storm surge analysis has been implemented by various previous studies (e.g., Lin et al., 2012; Marsooli et al. 2019). Also, Xu et al. (2020) used a similar method to estimate the wind field, and their estimated wind hazard based on the NCEP synthetic dataset compared well with historical wind observations in the Shanghai region.

2.4. Flood Probability Analysis

Statistical analysis is performed on the generated storm tides for locations/stations at 1000-m intervals along the Shanghai coast. The probability of storm tide events can be estimated by extreme value models such as generalized extreme value distribution family. In this study, the Generalized Pareto Distribution (GPD) is

202 applied to describe the limiting behavior of maximum storm tide values for all individual events using a
203 Peaks-Over-Threshold approach (Simiu and Heckert 1996) and the maximum likelihood method (Lin et al.,
204 2012). The GPD threshold is determined by trial to ensure that the smallest error in the distribution is obtained
205 (Marsooli et al., 2019). Then, the return periods of peak storm time levels are calculated by assuming that the
206 storm arrival for the region is a stationary Poisson process (Lin et al., 2012).
207
208 **2.5. Inland Inundation Modeling**
209
210 A well-established 2D hydraulic model (FloodMap-Inertial, Yu and Lane 2011) is utilized to derive coastal
211 flood inundation for each scenario. The model, as well as its earlier diffusion-based version (FloodMap, Yu
212 and Lane 2006a,b) have been tested and verified in a number of different environments (e.g., Tayefi et al.,
213 2007; Lane et al., 2008; Casas et al., 2010; Yin et al., 2013, 2016, 2019; Yu and Coulthard, 2015). It adopts a
214 simplified 2D solution to numerically solve the inertial form of the 2D shallow water equations by neglecting
215 the convective acceleration term in a raster-based domain. Inland flood routing takes the same structure as the
216 inertial algorithm of Bates et al. (2010), but with a slightly different method to calculate the time step. Rather
217 than using a global Courant–Freidrich–Levy Condition where the time step for the next iteration is calculated
218 based on the maximum water depth and velocity found at the last time step (e.g. Bates and De Roo, 2000), the
219 Forward Courant–Freidrich–Levy Condition (FCFL) approach described in Yu and Lane (2011) for the
220 diffusion-based version of FloodMap is used in the inertial model to maintain simulation stability and
221 minimize numerical diffusion.
222
223 To apply the model for inland flood simulation, two types of data are required: floodplain topography and

boundary conditions. In terms of the floodplain topography, a city-wide Digital Elevation Model (DEM) constructed from 0.5 m topographic contours is available (Yin et al., 2013), with a grid cell resolution of 50 m and a vertical accuracy of 0.1-0.2 m. The locations and heights of sea dikes along the coast, provided by Shanghai Water Authority (SWA), are then overlaid onto the original 'bare earth' DEM. An empirically-based uniform manning's n roughness coefficient of 0.06 is used in the simulation to represent the effect of urban features (e.g. buildings) on flood routing. For each synthetic storm, water level time series (every 30 minutes) at locations spaced at 1000 m intervals along the coast, derived from the ADCIRC model run, were used as flow boundary conditions to drive the flood modeling. The performance of the coupled ADCIRC-FloodMap method was investigated by Yin et al., (2016), where the ADCIRC-FloodMap method demonstrated higher efficiency and accuracy in inundation prediction at the city scale than using the ADCIRC model alone, which is particularly important for hazard modeling involving thousands of simulations.

3. Results and Discussions

3.1. Probabilistic Flood Hazards

For each location along the Shanghai coastline, the return periods of flood levels (storm tides) under the NCAR/NCEP current climate are estimated through the flood probability analysis. The spatially continuous distribution of the estimated flood levels with various return periods (10-, 100- and 1000-year) along the coast is presented in Fig. 1. Results indicate that the flood level substantially increases with the increase of return period: it is between 3.77 and 6.93 m (with an average value of 4.37 m above Wusong Datum) for the 10-year scenario, 4.57 and 8.48 m (5.19 m) for the 100-year scenario, and 5.88 and 12.10m (7.03 m) for the 1000-year scenario. The highest flood return levels (η) and the largest increases in η over the return periods can be

observed along the northern coast of Chongming Island. This spatially continuous distribution of simulated flood levels along the coast provides greater detail and accuracy for flood hazard assessment compared to a previous study (Yin et al., 2020), in which flood return levels were interpolated from sparsely distributed tide gauges.

Fig. 2 displays the flood return level curves at selected gauge stations estimated by our analysis, compared to estimates by SWA using the officially recommended Pearson-III distribution based on annual maximum values of recorded historical water levels. Similar to that shown in Fig. 1, the predicted flood return levels vary greatly from place to place along the coast. For example, the 1000-year flood height is about 7.76 m at Jinshan Station but only about 6.10 m at Luchaogang Station. Only very low-probability events (over 3000 ~ 10000 year) will exceed the crest levels of seawall. Results also show a large uncertainty in flood levels with long return periods (> 100 years). SWA's analysis predicts significantly higher flood levels, especially for small return periods (e.g., 5 ~ 6 m for the 10-year floods). Peak water levels recorded at the gauge stations during Typhoon Winnie indicate it to be close to a 100-year event by SWA's analysis but an 800 ~ 900-year event by our analysis. This discrepancy can be primarily attributed to the different distribution models and sample data used in the flood probability analyses. The occurrence of Typhoon Winnie may have contributed significantly to lifting the return level curves estimated based on the limited (less than 60 year) historical data. Otherwise, using limited-length historical data often underestimates extremes (Lin et al., 2014; Xu et al., 2020); extrapolating SWA's estimates for return periods greater than 1000 years would result in an underestimation of the extremes compared to our modeling-based estimates.

3.2. Worst-case Scenarios

The 5180 synthetic storm tide events simulated using ADCIRC are used as boundary conditions to drive inland flood modeling using FloodMap. Given the high level of floodwall protection, there are only a few storms that can cause inundation in Shanghai under the current sea level. Fig. 3a-c shows the spatial pattern of the storm tides and the resultant inundation footprints for three worst-case scenarios in Shanghai in the synthetic simulation under the NCAR/NCEP current climate condition. Typhoon A is a large sized storm that moves northwestward and makes landfall in Jinshan with a high intensity. Due to the wind field's asymmetry, the largest wind forces to the right of the track push surge into Yangtze River Estuary and produce the highest storm tide (over 9 m above Wusong Datum) at the northernmost end of Shanghai. Another relatively strong northwestward-moving storm (Typhoon B) makes landfall in Chongming and induces a comparable storm tide along the northern coast of the island. A smaller-size storm (Typhoon C) which makes landfall farther from the city also generates an extreme sea level during high tide in Hangzhou Bay (8.7 m above Wusong Datum) due to its higher intensity. The three worst-case scenarios have very low probabilities of occurrence (> 5000 years, based on their storm tide return period at the location of the maximum storm tide for each storm, shown by the black star in Fig. 3a-c) and are much higher than the largest storm tides in recorded history (6 ~ 7 m above Wusong Datum).

The synthetic events cause varying degrees of coastal flood inundation in Shanghai. The highest storm tides due to Typhoon A overwhelm low-lying and poorly-protected coastal floodplains and islands in the Yangtze River Estuary (Fig. 3a). When subject to Typhoon B induced coastal flooding, the inundation area covers about 564 km^2 in the northeastern part of Chongming Island (Fig. 3b). Particularly, the waterfront areas of western (Typhoon A) and eastern (Typhoon B) Chongming are flooded with maximum water depths higher

than 3 m. In contrast, only marginal inundations with shallow water depth (mostly lower than 0.5 m) are observed in the coastal region along Hangzhou Bay under the Typhoon C scenario (Fig. 3c). This relatively small inundation depth can be explained by the presence of lateral topographic confinement and the relatively high crest heights of the seawalls (7 ~ 8 m above Wusong Datum). Pudong New Area and Changxing Island appear to be immune to these extreme flood scenarios, because of their high standard seawalls (8 ~ 11 m above Wusong Datum) and comparatively low storm tides in the lower Yangtze River Estuary. Mainland Shanghai seems to be generally safe from the storm-induced flooding except a small portion of dike-protected hinterland in Baoshan (Fig. 3a). The results presented here highlight the vulnerability of the areas in the upper Yangtze River Estuary where larger storm tides develop and which have relatively low levels of seawall protection, such as Chongming Island and Baoshan.

3.3. SLR impact on flooding

Yin et al. (2020) provided the probabilistic SLR projections for Shanghai, which take into account both climatic and non-climatic (subsidence) components, under three Representative Concentration Pathways (RCP 2.6, 4.5 and 8.5) by the end of 21st century, relative to the baseline year of 2010. The median (50th percentile) estimates under RCP 8.5 are used here to investigate the effect of local relative SLR on typhoon-induced coastal flooding and inundation. We find that the projected SLR would lead to non-linear impact on flood and inundation hazards. For example, the 3000-year flood level at the Jinshan station (at the height of the seawall to cause inundation) would become a less than 1000- and 900-year flood events in the mid- and end-of-twenty-first century, respectively (Fig. 2). Overall in Shanghai, compared with the current situation, typhoon-induced flood inundation would occur two times more frequently with a 0.5-m SLR by 2050 and 20

313 times more frequently with a 1.36-m SLR by 2100.

314

315 Inundation severity will also significantly increase. Fig. 3d-i display the derived coastal flood inundations for
316 the three worst-cases under the 2050 and 2100 sea levels. A cross comparison between Fig. 3a-c and Fig. 3d-i
317 reveals that extreme typhoon-induced coastal inundations in Shanghai, as expected, would increase
318 significantly under SLR. Although the general patterns of inundation are characterized by a certain degree of
319 consistency between the current and 2050 scenarios, the flooded areas are projected to increase by 26%, 24%,
320 and 437% for Typhoon A, B and C, respectively. Meanwhile, the projected SLR of 0.5 m could contribute to a
321 23%, 19% and 74% rises in the average inundation depth for the three cases, respectively. If the local sea level
322 is raised by 1.36 m by the end of the century, the predicted inundation areas for Typhoon A, B, and C will be
323 respectively 60%, 110% and 1360% larger than those with the present-day sea level, and the average
324 inundation depth will increase respectively by 69%, 16% and 141%. Extreme flood hazards caused by
325 Typhoon A and B would almost totally inundate the Chongming and Hengsha islands by 2100. Without an
326 upgraded flood defense, Baoshan and the coastal districts along Hangzhou Bay could also be greatly affected
327 by Typhoon A and C under the 2100 SLR.

328

329 **4. Conclusions**

330

331 In this work, we develop a combined hurricane-circulation-inundation model to quantify extreme coastal
332 flooding induced by synthetic storms under current and future sea levels in Shanghai, China. The main
333 conclusions are summarized as follows: 1) although the storm tide hazard is high, Shanghai's flood protection
334 system is sufficient for preventing majority of the city from severe flooding (> 100 years) from storm tide

under the current climate; 2) extreme "worst-case" scenarios (> 5000 years) can generate unprecedented storm tides (8 - 9 m) in Yangtze River Estuary or Hangzhou Bay, even under the current climate; 3) future SLR will greatly increase Shanghai's flooding risk compared to the current state, with inundation two times and 20 times more likely to occur by mid- and late-21st century, respectively, and inundation depth and area to greatly increases (e.g., 60-1360% increase in the inundation area for the "worst cases" by 2100).

The present study contributes to a better understanding of extreme coastal flooding from TC-induced storm tide and SLR in Shanghai and unlocks the potential for estimating flood hazard evolution due to SLR as well as storm change (e.g., Marsooli et al., 2019) in a changing climate. The methodology is applicable to any coastal city that is susceptible to TC surge flooding and rising sea level. However, since we neglect wave effects on the water level, major seawall failure mechanisms such as wave overtopping and breaching are not considered in the present storm flood modeling; the inundation risk estimated herein is likely a lower bound. Further work will include wave modeling and dike reliability analysis (e.g., Yin et al., 2020) in the climatological-hydrodynamic modeling to better quantify the flood risk under both the current and future climate conditions.

Acknowledgments

This paper was supported by the National Key Research and Development Program of China (Grant no: 2018YFC1508803, 2017YFE0107400, 2017YFE0100700), the National Natural Science Foundation of China (Grant no: 41871164, 51761135024), the Fundamental Research Funds for the Central Universities (Grant no: 2018ECNU-QKT001, 2017ECNUKXK013), the Institute of Eco-Chongming (Grant no: ECNU-IEC-202001), and the National Science Foundation of the United States (grant EAR-1520683). We also thank Professor Kerry Emanuel (MIT) for generating the synthetic TC dataset and Professor Jianrong Zhu (ECNU) for providing us with the high-resolution bathymetry data. Data is available through Xu et al. 2020 and Yin et al. 2020. Model simulations presented in this study are available for download through DOI 10.6084/m9.figshare.12911630.

References

Aerts J C, Lin N, Botzen W J, Emanuel K, Moel H, 2013. Low-probability flood risk modeling for New York City, Risk Analysis, 33: 772-788.

Barnard, P.L., Erikson, L.H., Foxgrover, A.C., Hart, J.A.F., Limber, P., O'Neill, A.C., van Ormondt, M., Vitousek, S., Wood, N., Hayden, M.K., Jones, J.M., 2019. Dynamic flood modeling essential to assess the coastal impacts of climate change. Scientific Reports, 9: 4309.

Bates P D, De Roo A P J, 2000. A simple raster-based model for flood inundation simulation. Journal of Hydrology, 236: 54-77.

Bates P D, Horritt M, Fewtrell T, 2010. A simple inertial formulation of the shallow water equations for efficient two-dimensional flood inundation modelling. Journal of Hydrology, 387(1-2): 33-45.

Batts M E, Cordes M R, Simiu E, 1980. Sampling errors in estimation of extreme hurricane winds. Journal of the Structural Division-ASCE, 106: 2109-2115.

Blake E S, Kimberlain T B, Berg R J, Cangialosi J P, Beven J L, 2013. Tropical cyclone report hurricane sandy (Rep. AL182012). Miami, FL: National Hurricane Center.

Bretschneider C, 1972. A non-dimensional stationary hurricane wave model. Paper presented at Offshore Technology Conference, Hous- ton, TX (Pap. OTC 1517).

Casas A, Lane, S N, Yu D, Benito G, 2010. A method for parameterising roughness and topographic sub-grid effects in hydraulic modeling from LiDAR data. Hydrology and Earth System Sciences, 14 (8): 1567-1579.

Egbert G D, Erofeeva S Y, 2002. Efficient inverse modeling of barotropic ocean tides. Journal of Atmospheric and Oceanic Technology, 19: 183-204.

Emanuel K, Sundararajan R, Williams J, 2008. Hurricanes and global warming: Results from downscaling IPCC AR4 simulations. Bulletin of the American Meteorological Society, 89: 347-368.

Emanuel K A, Rotunno R, 2011. Self-stratification of tropical cyclone outflow. Part I: Implications for storm structure. Journal of Atmospheric Sciences, 68: 2236-2249.

Emanuel K A, 2013. Downscaling CMIP5 climate models shows increased tropical cyclone activity over the 21st century. Proceedings of the National Academy of Sciences of United States of America, 110(30): 12219-12224.

Georgiou P N, Davenport A G, Vickery P J, 1983. Design wind speeds in regions dominated by tropical cyclones. Journal of Wind Engineering and Industrial Aerodynamics, 13: 139-152.

Hallegatte S, Green C, Nicholls R J, Corfee-Morlot J, 2006. Future flood losses in major coastal cities. Nature Climate Change, 3: 802-806.

Holland G J, 1980. An analytical model of the wind and pressure profiles in hurricanes. Monthly Weather Review, 108(8): 1212-1218.

Jelesnianski C P, Chen J, Shaffer W A, 1992. SLOSH: Sea, lake, and overland surges from hurricanes.

Jing R, Lin N, 2020. An environment−dependent probabilistic tropical cyclone model. Journal of Advances in Modeling Earth Systems, 12: e2019MS001975.

Kalnay E, Kanamitsu M, Kistler R, Collins W, Deaven D, Gandin L, Iredell M, Saha S, White G, Woollen J, Zhu Y, Leetmaa A, Reynolds R, Chelliah M, Ebisuzaki W, Higgins W, Janowiak J, Ropelewski K, Wang J, Jenne R, Dennis J, 1996. The NCEP/NCAR 40-year reanalysis project. Bulletin of American Meteorological Society, 77 (3): 437-471.

Kates R W, Colten C E, Laska S, Leatherman S P, 2006. Reconstruction of New Orleans after Hurricane

Katrina: A research perspective. Proceedings of the National Academy of Sciences of United States of America, 103: 14653-14660.
Knutson T , Camargo S J, Chan J C L, Emanuel K, Ho C-H, Kossin J, Mohapatra M, Satoh M, Sugi M, Walsh K, Wu L, 2020. Tropical Cyclones and Climate Change Assessment: Part II: Projected Response to Anthropogenic Warming. Bulletin of the American Meteorological Society, 101(3): E303–E322.
Lane S N, Reid S C, Tayefi V, Yu D, Hardy R J. Reconceptualising coarse sediment delivery problems in rivers as catchment-scale and diffuse. Geomorphology, 2008, 98(34): 227-249.Lin N, Emanuel K A, Smith J A, Vanmarcke E, 2010. Risk Assessment of Hurricane Storm Surge for New York City. Journal of Geophysical Research, 115: D18121.
Lee C Y, Tippett M K, Sobel A H, Camargo S J, 2018. An environmentally forced tropical cyclone hazard model. Journal of Advances in Modeling Earth Systems, 10, 223-241.
Lin N, Emanuel K A, Smith J A, Vanmarcke E, 2010. Risk Assessment of Hurricane Storm Surge for New York City. Journal of Geophysical Research, 115 (D18): D18121.
Lin N, Chavas D, 2012. On hurricane parametric wind and applications in storm surge modeling. Journal of Geophysical Research, 117: D09120.
Lin N, Lane P, Emanuel K A, Sullivan R M, Donnelly J P, 2014. Heightened hurricane surge risk in northwest Florida revealed from climatological-hydrodynamic modeling and paleorecord reconstruction. Journal of Geophysical Research, 119(14): 8606-8623.
Lin N, Emanuel K, Oppenheimer M, Vanmarcke E, 2012. Physically based assessment of hurricane surge threat under climate change. Nature Climate Change, 2: 462-467.
Lin N, Shullman E, 2017. Dealing with Hurricane Surge Flooding in a Changing Environment: Part I. Risk Assessment Considering Storm Climatology Change, Sea Level Rise, and Coastal Development. Stochastic Environmental Research and Risk Assessment, 31: 2379-2400.
Lin N, Kopp R E, Horton B P, Donnelly J P, 2016. Hurricane Sandy's Flood Frequency Increasing from Year 1800 to 2100. Proceedings of the National Academy of Sciences of the United States, 113 (43): 12071-12075.
Luettich R A, Westerink J J, Scheffner N W, 1992. ADCIRC: An advanced three-dimensional circulation model for shelves, coasts and estuaries. Report 1. Theory and methodology of ADCIRC-2DDI and ADCIRC-3DL (Tech. Rep. DRP-92-6). Vicksburg, MS: U.S. Army Corps of Engineers.
Marsooli R, Lin N, 2018. Numerical modeling of historical storm tides and waves and their interactions along the U.S. east and Gulf Coasts. Journal of Geophysical Research: Oceans, 123: 3844-3874.
Marsooli R, Lin N, Emanuel K, Feng K. Climate change exacerbates hurricane flood hazards along US Atlantic and Gulf Coasts in spatially varying patterns. Nature Communications, 2019, 10: 3785.
Melet, A., Meyssignac, B., Almar, R., Le Cozannet, G., 2018. Under-estimated wave contribution to coastal sea-level rise. Nature Climate Change, 8(3), 234–239. doi:10.1038/s41558-018-0088-y
Powell M D, Houston S H, Reinhold T A, 1996. Hurricane Andrew's landfall in South Florida. Part I: standardizing measurements for documentation of surface wind fields. Weather Forecast. 11: 304-328.
Resio, D.T., Westerink, J.J., 2008. Modeling the physics of storm surges. Physics Today, 61(9), 33–38. doi:10.1063/1.2982120
Simiu E, Heckert N A. Extreme wind distribution tails: a peak over threshold approach. Journal of Structural Engineering (ASCE), 1996, 122: 539-547.
Smith A B, Katz R W. US billion-dollar weather and climate disasters: Data sources, trends, accuracy and biases. Natural Hazards, 2013, 67: 387-410.

448 Tayefi V, Lane S N, Hardy R J, Yu D. A comparison of one- and two-dimensional approaches to modelling
449 flood inundation over complex upland floodplains. Hydrological Processes, 2007, 21(23): 3190-3202.
450 Vitousek, S., Barnard, P.L., Fletcher, C.H., Frazer, N., Erikson, L., Storlazzi, C.D., 2017. Doubling of coastal
451 flooding frequency within decades due to sea-level rise. Scientific Reports, 7: 1399. doi:10.1038/s41598-
452 017-01362-7
453 Vickery P J, Skerjl P F, Twisdale L A, 2000. Simulation of hurricane risk in the U.S. using empirical track
454 model. Journal of Structural Engineering, 126: 1222-1237.
455 Vickery P J, Wadhera D, Twisdale L A Jr, Lavelle F M, 2009. U.S. hurricane wind speed risk and uncertainty.
456 Journal of Structural Engineering, 135: 301-320.
457 Wang J, Huang H, Zhang C, Liu J, Yan J, Geng L, 2017. The preventive measures to deal with the disaster of
458 storm surge of Shanghai city. Ocean Development and Management, 2017, 34(1):92-96. (In Chinese)
459 Westerink J J, Luettich R A, Blain C A, Scheffner N W, 1994. ADCIRC: An advanced three-dimensional
460 circulation model for shelves, coasts and estuaries. Report 2: Users' manual for ADCIRC-2DDI (Tech.
461 Rep. DRP-92-6). Vicksburg, MS: U.S. Army Corps of Engineers.
462 Westerink J J, Luettich R A, Feyen J C, Atkinson J H, Dawson C, Roberts H J, Powell M D, Dunion J P,
463 Kubatko E J, Pourtaheri H, 2008. A basin- to channel-scale unstructured grid hurricane storm surge
464 model applied to Southern Louisiana. Monthly Weather Review, 136(3), 833-864.
465 Woodruff J D, Irish J L, Camargo S J, 2013. Coastal flooding by tropical cyclones and sea-level rise. Nature,
466 504: 44-52.
467 Xian S, Yin J, Lin N, Oppenheimer M, 2018. Influence of Risk Factors and Past Events on Flood Resilience
468 in Coastal Megacities: Comparative Analysis of NYC and Shanghai. Science of the Total Environment,
469 2018, 610-611C: 1251-1261.
470 Xu H, Lin N, Huang M, Lou W, 2020. Design tropical cyclone wind speed when considering climate change.
471 ASCE Journal of Structural Engineering, 146(5): 04020063.
472 Yin J, Yu D P, Yin Z E, Wang J, Xu S Y, 2013. Modelling the combined impacts of sea-level rise and land
473 subsidence on storm tides induced flooding of the Huangpu River in Shanghai, China. Climatic Change,
474 2013, 119(3): 919-932.
475 Yin J, Yu D P, Yin Z E, Wang J, Xu S Y, 2015. Modelling the anthropogenic impacts on fluvial flood risks in
476 a coastal mega-city: A scenario-based case study in Shanghai, China. Landscape and Urban Planning,
477 136: 144-155.
478 Yin J, Lin N, Yu D. Coupled modeling of storm surge and coastal inundation: a case study in New York City
479 during Hurricane Sandy. Water Resources Research, 2016, 52: 8685-8699.
480 Yin J, Zhao Q, Yu D, Lin N, Kubanek J, Ma G, Liu M, Pepe A. Long-term flood-hazard modeling for coastal
481 areas using InSAR measurements and a hydrodynamic model: the case study of Lingang New City,
482 Shanghai. Journal of Hydrology, 2019, 571: 593-604.
483 Yin J, Jonkman S, Lin N, Yu D, Aerts J, Wilby R, Pan M, Wood E, Bricker J, Ke Q, Zeng Z, Zhao Q, Ge J,
484 Wang J. Flood risks in sinking delta cities: time for a re-evaluation? Earth's Future, 2020, 8:
485 e2020EF001614.
486 Yu D, Lane S N, 2006a. Urban fluvial flood modelling using a two-dimensional diffusion wave treatment,
487 part 1: mesh resolution effects. Hydrological Processes, 20: 1541-1565.
488 Yu D, Lane S N, 2006b. Urban fluvial flood modelling using a two-dimensional diffusion wave treatment,
489 part 2: development of a sub grid-scale treatment. Hydrological Processes, 20: 1567-1583.
490 Yu D, Lane S N, 2011. Interaction between subgrid-scale resolution, feature representation and grid-scale

resolution in flood inundation modelling. Hydrological Processes, 25: 36-53.
Yu D, Coulthard T J, 2015. Evaluating the importance of catchment hydrological parameters for urban surface water flood modelling using a simple hydro-inundation model. Journal of Hydrology, 524: 385-400.
Zhu J, Bao D, 2016. The effects of river regime changes in the Changjiang Estuary on hydrodynamics and salinity intrusion in the past 60 years I. River regime changes. Haiyang Xuebao, 2016, 38(12): 11-22. (In Chinese)

Figure Captions

Fig. 1 Estimated storm tide levels (m above Wusong Datum) along the Shanghai region coast for 10- (a), 100- (b) and 1000-year (c) return periods under the current climate.

Fig. 2 Estimated flood return period curves at six selected gauge stations around Shanghai for the NCAR/NCEP current climate (black) and 2050 (0.5 m; orange) and 2100 (1.36 m; purple) sea levels. The x axis is the return period (year) and the y axis is the flood level (m above Wusong Datum). The shade area represents the 95% confidence interval. The green line represents the crest level of seawall at the gauge stations. The red line represents the peak water level recorded at gauge stations during Typhoon Winnie. The blue dot represents the flood return period level estimated by SWA using a Pearson-III distribution based on annual maximum values of recorded historical water levels at the gauge stations.

Fig. 3 Three worst-case coastal flood inundation scenarios in Shanghai. (a-c) Typhoon A, B and C induced coastal inundations under the current climate; (d-f) Typhoon A, B and C induced coastal inundations under the 2050 sea level (0.5 m); (g-i) Typhoon A, B and C induced flood inundations under the 2100 sea level (1.36 m). The black curve in the insert shows the storm track and the black star shows the location with the maximum water level during the storm (a, b, c). The storm parameters at landfall are: (a, d, g) Typhoon A: maximum wind speed V_m = 46.9 m/s, minimum sea-level pressure P_c = 958.8 mb, radius of maximum wind R_m = 81.2 km, and translation speed U_t = 13.4 m/s; (b, e, h) Typhoon B: V_m = 51.0 m/s, P_c = 952.4 mb, R_m = 80.1 km, and U_t = 9.0 m/s; (c, f, j) Typhoon C: V_m = 52.0 m/s, P_c = 951.5 mb, R_m = 63.7 km, and U_t = 6.7 m/s.

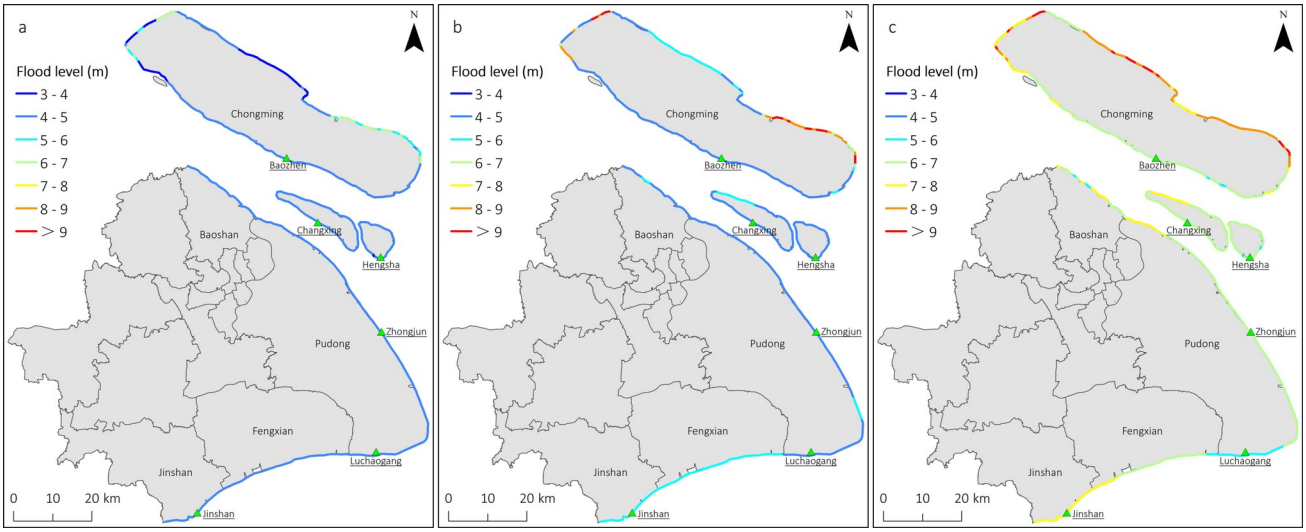
a
b
c
N
Flood level (m)
3 - 4
4 - 5
5 - 6
6 - 7
7 - 8
8 - 9
> 9
Chongming
Baozhen
Changxing
Hengsha
Baoshan
Zhongjun
Pudong
Fengxian
Luchaogang
Jinshan
0 10 20 km

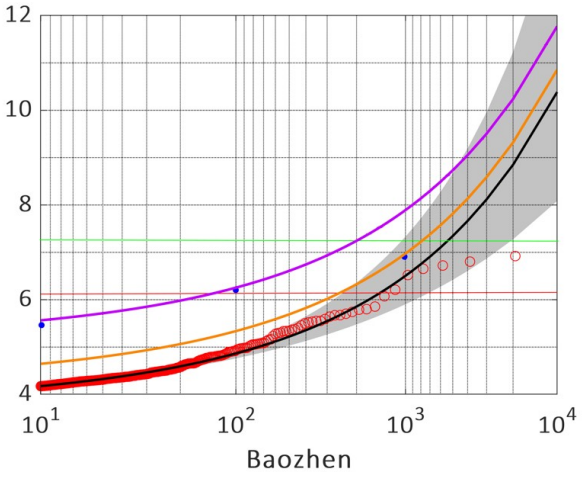

Baozhen

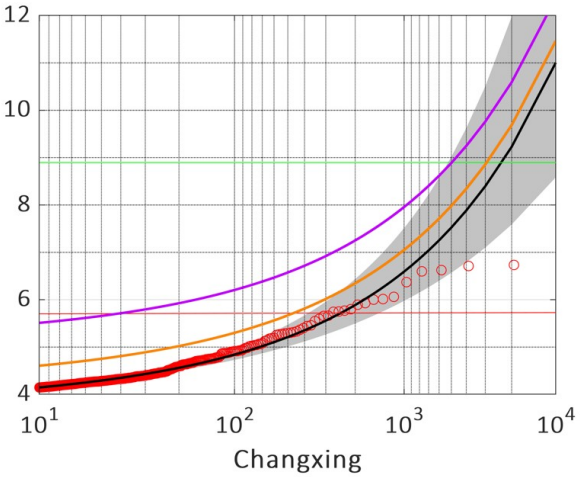

Changxing

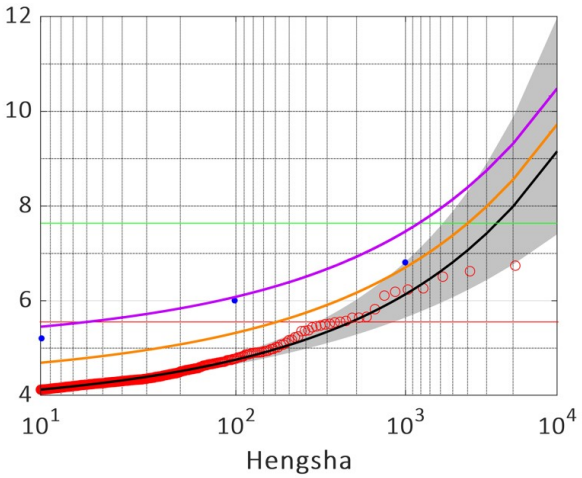

Hengsha

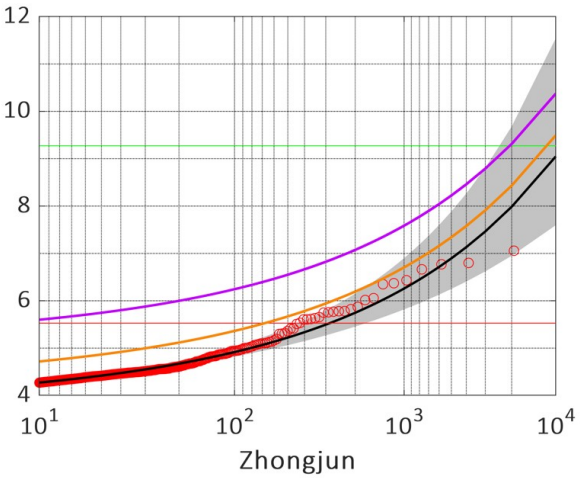

Zhongjun

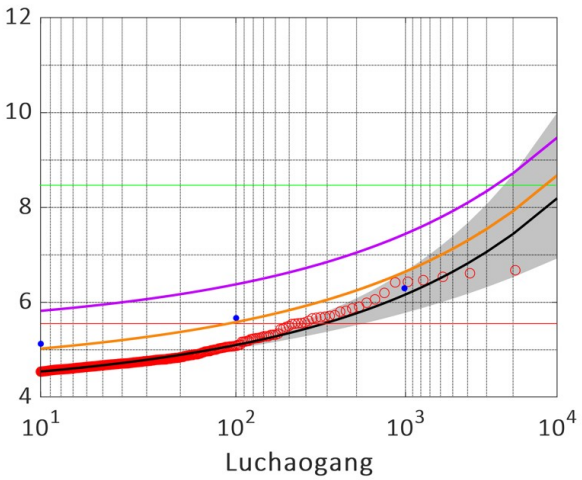

Luchaogang

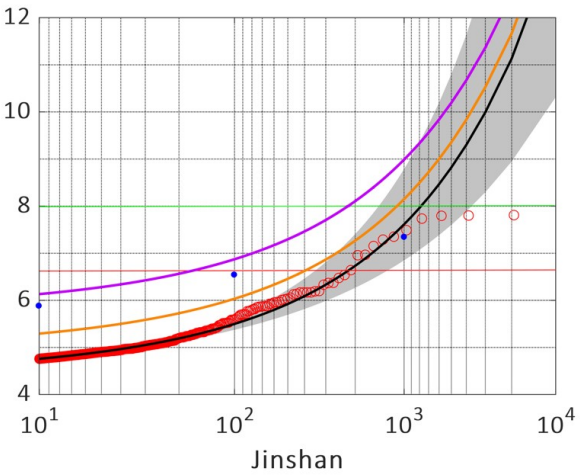

Jinshan

545

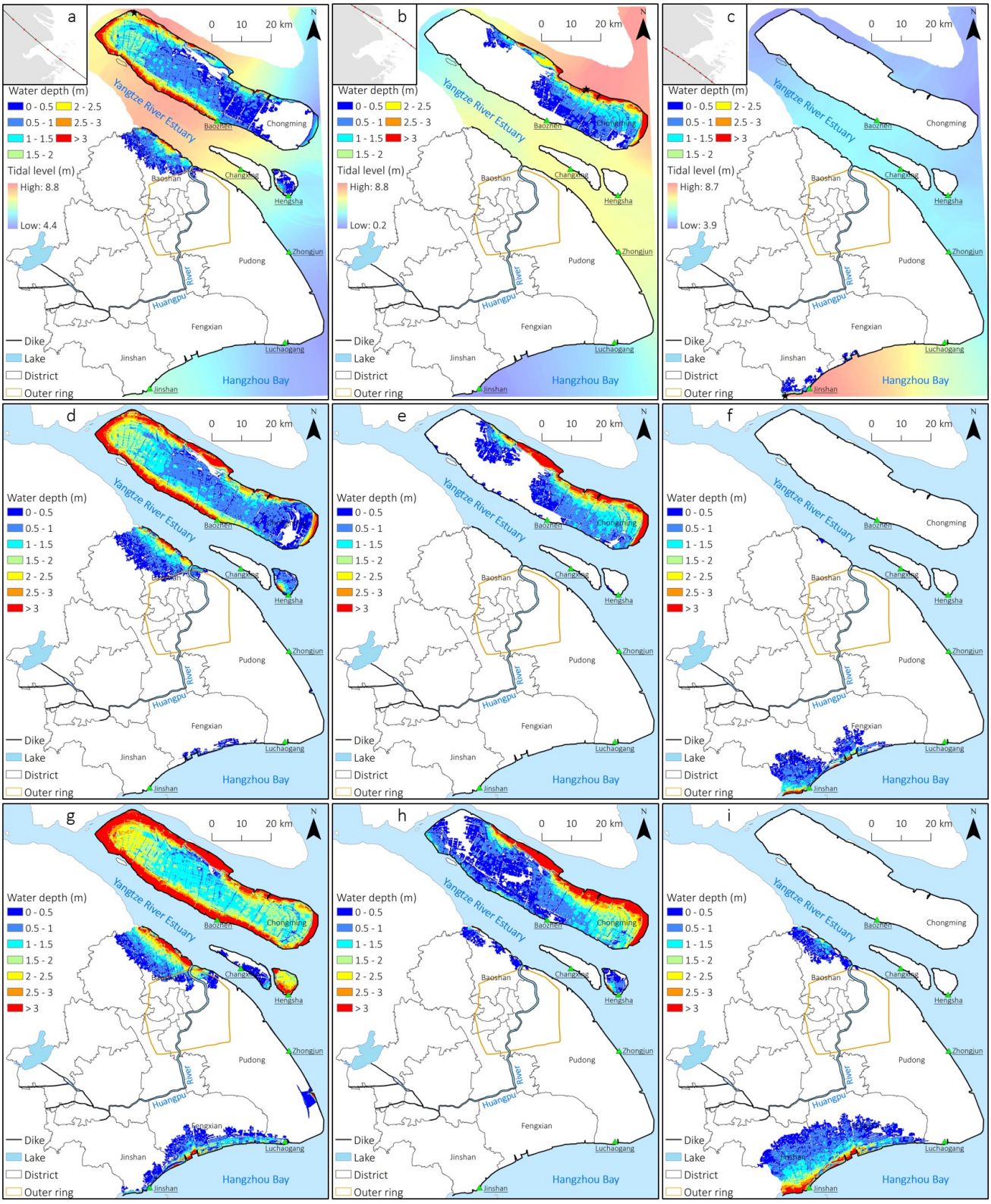
a
b
c
d
e
f
g
h
i
0 10 20 km
N
Water depth (m)
0 - 0.5
0.5 - 1
1 - 1.5
1.5 - 2
2 - 2.5
2.5 - 3
> 3
Tidal level (m)
High: 8.8
Low: 4.4
High: 8.8
Low: 0.2
High: 8.7
Low: 3.9
Yangtze River Estuary
Baoshan
Chongming
Changxing
Hengsha
Zhongjun
Pudong
Huangpu River
Fengxian
Jinshan
Luchaogang
Dike
Lake
District
Outer ring
Hangzhou Bay

546